symmetry

MDPI

Article

Influence of Parametric Symmetry on the Dynamics of 3D Sinusoidal Discrete Systems

Karthikeyan Rajagopal [1,†], Sathiyadevi Kanagaraj [1,†], Christos Volos [2,*] and Anitha Karthikeyan [3,†]

[1] Centre for Nonlinear Systems, Chennai Institute of Technology, Chennai 600069, India
[2] Laboratory of Nonlinear Systems, Circuits & Complexity, Physics Department, Aristotle University of Thessaloniki, 54124 Thessaloniki, Greece
[3] Department of Electronics and Communication Engineering, Vemu Institute of Technology, Chitoor 517112, India
* Correspondence: volos@physics.auth.gr
† These authors contributed equally to this work.

Abstract: The discrete system serves an important role in mimicking collective dynamics found in continuous dynamical systems, which are relevant to many realistic natural and artificial systems. To investigate the dynamical transition of a discrete system, we employ three-dimensional sinusoidal discrete maps with an additional self feedback factor. Specifically, we focus on dynamical transitions with respect to the bifurcation parameter, sine function amplitude, and intensity of self feedback factors. We demonstrate the presence of symmetry in relation to parametric variation using two parameter diagrams. The study is then expanded to the network of sine maps in the presence of self-feedback factor. We discover that negative feedback exhibits the transition from cluster state to synchronization while raising the coupling strength for small-world network interactions. Furthermore, increasing feedback from negative to positive causes the transition from synchronization to desynchronization via chimera state for various complex network connectivities.

Keywords: sine maps; bifurcation; chimera; synchronization

Citation: Rajagopal, K.; Kanagaraj, S.; Volos, C.; Karthikeyan, A. Influence of Parametric Symmetry on the Dynamics of 3D Sinusoidal Discrete Systems. *Symmetry* **2023**, *15*, 780. https://doi.org/10.3390/sym15040780

Academic Editor: Vladimir García-Morales

Received: 19 January 2023
Revised: 16 March 2023
Accepted: 20 March 2023
Published: 23 March 2023

1. Introduction

In realistic situations, many natural and artificial systems can exhibit a wide range of complex behaviors such as chaos, hyperchaos, strange nonchaos, and so on [1–5]. Each of the dynamical behaviors has numerous applications in the fields of computer science and technology, engineering, and telecommunications, among others. To comprehend such complex behavior, distinct discrete and continuous systems have been modeled so far. For instance, Edward Lorenz originally proposed the chaotic continuous-time system to understand chaotic dynamics [6]. Following that, various chaotic and hyperchaotic continuous-time systems such as Rössler, Sprott, and many others have been developed [7–9]. Chaotic circuits based on memristor-memcapacitors and their fractional order circuit have been implemented to demonstrate the complex behaviours [10,11]. These dynamics are not restricted to continuous systems; they can occur in discrete-time systems as well.

Moreover, the discrete system can be found in many research fields, including image encryption [12,13], neural networks [14], viscoelastic materials [15], random signal generator [16], biological mechanism [17], system control [18], and so on. Robert May introduced the Logistic map in 1976 to demonstrate the chaotic dynamics in a discrete system [19]. Following that, several discrete systems were developed to study the chaotic and hyperchaotic dynamics. In particular, the existence of chaos and discrete chaos have been reported through the Henon map, Chebyshev Hyperchaotic Map and its fractional form [20–22]. Using the generalized Henon maps, the existence of higher dimensional chaotic and hyperchaotic dynamics have been delineated in [23]. Chen proposed the 3D chaotic cat maps to encrypt the image by implementing confusion between the cipher-image and the plain-image application with real-time image encryption via internet and transmission applications [24]. The transition from periodic to chaotic dynamics has been identified in a 1D piecewise linear as well as nonlinear chaotic maps [25,26]. Pseudo-random number generation has been achieved by utililzing adaptive Zaslavsky map under multi-parametric bifurcation analysis [27]. The existence of many hidden attractors has been illustrated using fractional hyper chaotic maps [28]. In a stochastic discrete ecosystem, control analysis and equilibrium points with symmetry are defined [29]. It has been discovered that the discrete memristor-based coupling model may enhance the complexity of discrete systems such as the Logistic map and a Sine map (MCLS), which have applications in information encryption [30]. It has also been noted that the change in system symmetry is seen during the transition from continuous to discrete system [31].

Sinusoidal or sine maps, on the other hand, are intriguing in mathematics, physics, and biology since they are typically used to represent the many oscillatory processes that occur in such systems. It may also be used to describe the recurring patterns seen in natural systems such as ocean waves, light waves, and sound waves, among others. The occurrence of chaotic resonance has been delineated using sine circle maps [32]. Then the random bit generation has been demonstrated by considering chaotic two-dimensional sine discrete maps [33]. The prediction of bifurcation points that occur via period-doubling phenomena has been illustrated through two different chaotic maps namely the symmetric sine map and Gaussian map [34]. Through fractional order, chaotic maps with trigonometric sine functions can exhibit multi-fold strange attractors to chaos through a period-doubling bifurcation [35]. The existence of complex and chaotic dynamics of logistic sine square maps have been discussed in [36]. In addition, using delayed sine map which is developed by using a linear-delay-modulation method for developing the encryption algorithm to develop confusion-diffusion architecture [37]. Application with the secure communications, 2D infinite collapse sine model has been implemented to show the existence of complex hyperchaotic dynamics [38]. The impact of discrete memristive chaotic sine maps are implemented and identified such discrete memristor can enhance the characteristics of chaotic dynamics and its security is higher than other chaotic maps [39].

Furthermore, the analysis has been expanded to incorporate the coupled version of maps. The control of bistability has been reported by developing the parametrically coupled network of sine maps [40]. The simultaneous presence of chaotic synchronization and chaotic antisynchronization has been noticed in coupled sine maps and spatial synchronization with temporal periodic solution has been delineated in coupled sine circle maps [41,42]. Through a system of coupled maps, routes to the crisis, bifurcation transitions, and dimension variability are also detailed, followed by, spatial and spatio-temporal intermittency has been revealed in [43]. Further, suppression of chaos has been noticed by nonlinearly coupled sine square maps [44]. The transition from unsynchronization to synchronization was observed when the coupling scheme of the lattice of sine-circle maps was changed from global to local, and the transition between dynamical states has been recognized by plateau size [45]. The existence of various spiral wave patterns including quasi-periodic, periodic, and banded spiral waves with polygonal shapes was reported in a 2D lattice of sine circle maps [46]. Motivated by the preceding analysis on discrete systems, particularly sine maps, we consider the three-dimensional sine maps with additional self-feedback. We examine the impact of various parameters including the bifurcation parameter, amplitude of sinusoidal function as well as the strength of self-feedback since it is not well explored in the literature. In particular, we show the existence of hyperchaos when increasing the feedback parameter from negative to positive magnitudes. Eventually, we show the existence of symmetric patterns in the dynamical transitions among the periodic, quasiperiodic, and chaotic dynamics when varying bifurcation parameter or amplitude of sinusoidal force. Additionally, the transition from desynchronization to synchronisation via the cluster state are revealed in a network of sine maps when changing coupling strength. The dynamical transition of the proposed network under consideration is also investigated using a variety of connecting topologies and an increasing feedback parameter for a fixed coupling strength.

The remaining sections of the article are as follows: 3D discrete-time sinusoidal map is introduced in Section 2. The corresponding dynamical transitions with respect to distinct parameters including the bifurcation parameter, the amplitude of sine maps, and self-feedback factors are discussed in Section 3. Furthermore, the symmetric patterns in parameter spaces are detailed in Section 4. The network behavior of coupled sine maps is further illustrated in Section 5. Finally, the observed results are summarized in Section 6.

2. Model of 3D Sinusoidal Discrete Maps

Mammery used 3D sine maps [47], to investigate the existence of chaos and its transition mechanism. We considered 3D sine maps with two nonlinear sinusoidal functions, similar to the map used previously. In addition, we introduced the self-feedback parameter to investigate its impact on previously observed complex behaviors. The expression for a 3-dimensional sinusoidal discrete map with the self-feedback term can be written as,

$$\begin{aligned} x_{j+1} &= y_j, \\ y_{j+1} &= sin(z_j), \\ z_{j+1} &= \alpha + \beta x_j + \gamma y_j - \delta sin(z_j) + \mu z_j. \end{aligned} \tag{1}$$

where α, β, and γ, are the bifurcation parameters. δ is the amplitude of the sine function. x_j, y_j and z_j are the state variables. μ is the feedback strength. The parameter values are fixed as $\alpha = -3.76$, $\beta = 0.9$, $\gamma = 0.9$, $\delta = 1$ and $\mu = 0.01$, unless otherwise specified.

3. Dynamical Transitions: Bifurcation Analysis and Lyapunov Exponents

Initially, the dynamical transitions of the system (1) are investigated using a bifurcation diagram by finding the local maxima of the z-variable. We discover that the occurrence of regular recurring symmetric patterns with the transition from periodic to chaotic and vice versa can occur as a function of the bifurcation parameter α, as shown in Figure 1a. The magnitude of α, in particular, enhances the amplitude of the attractors in the patterns. The repeating chaotic and periodic regions are visible in the LEs, with the periodic region having all negative LEs and the chaotic region having one LE or two positive LEs, implying the presence of chaotic or hyperchaotic attractors.

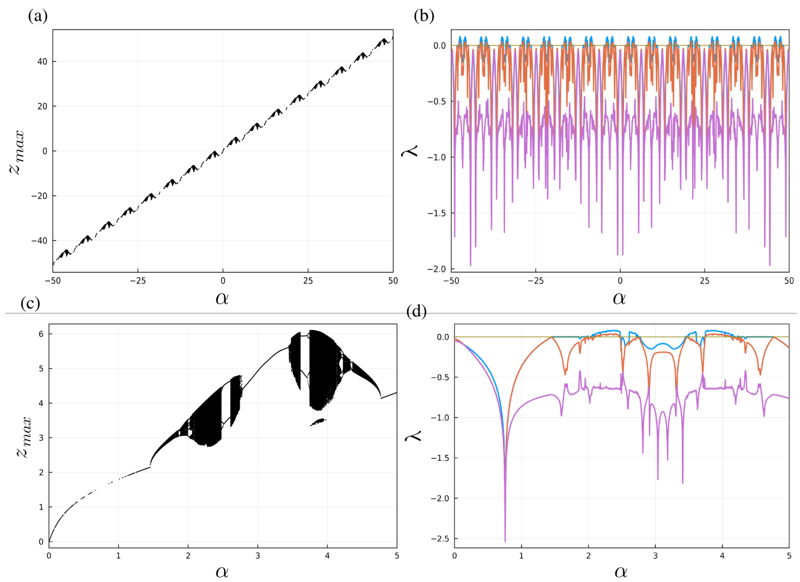

Figure 1. (**a**) Bifurcation diagram of the system (1) as a function of α, for ranges between -50 to $+50$, and (**b**) the corresponding Lyapunov exponents (LEs). (**c**,**d**) are a zoomed-in view of a portion of the bifurcation diagram and the associated LEs.

To gain a better understanding of the attractor transitions, we plotted a zoomed-in view of a small part of the bifurcation transition from Figure 1a in Figure 1c. By comparing the bifurcation transition shown in Figure 1c with the LE shown in Figure 1d, we discovered that the presence of periodic (P) attractors at lower values of $\alpha \in [0, 1.455]$ where all the LE are negative. We discovered the transition to a quasi-periodic (QP) attractor in the range $\alpha \in [1.456, 1.990]$ by increasing the magnitude of α. In this region, we discovered that one LE has a value of zero, while the other two have negative values. When the bifurcation parameter $\alpha \in [1.991, 2.461]$ is increased, hyperchaos (HC) occurs, with two LE being positive. Furthermore, the swing of periodic attractors via chaotic (CH) attractors is observed as varying the magnitude of α. The range of bifurcation parameters takes the values $\alpha \in [2.462, 2.61]$ for periodic, $\alpha \in [2.62, 2.711]$ for chaotic attractor and $\alpha \in [2.712, 3.493]$ for periodic attractors, respectively. The presence of a chaotic attractor in the above-mentioned range of α is confirmed by LE, with one LE displaying positive values and the other showing negative values. As the value of α increases, the reflection symmetry in the dynamical transition becomes visible. The following are the parameter ranges for each region: $\alpha \in [2.712, 3.492]$ for P $\rightarrow$ $\alpha \in [3.493, 3.607]$ for CH $\rightarrow$ $\alpha \in [3.608, 3.747]$ for P $\rightarrow$ $\alpha \in [3.748, 4.163]$ for HC $\rightarrow$ $\alpha \in [4.164, 4.763]$ for QP $\rightarrow$ $\alpha \in [4.764, 5.0]$ for P. From the aforementioned findings, it is noticeable that the existence of reflection symmetry among the dynamical transitions and the observed transitions reoccur over a wide set of α.

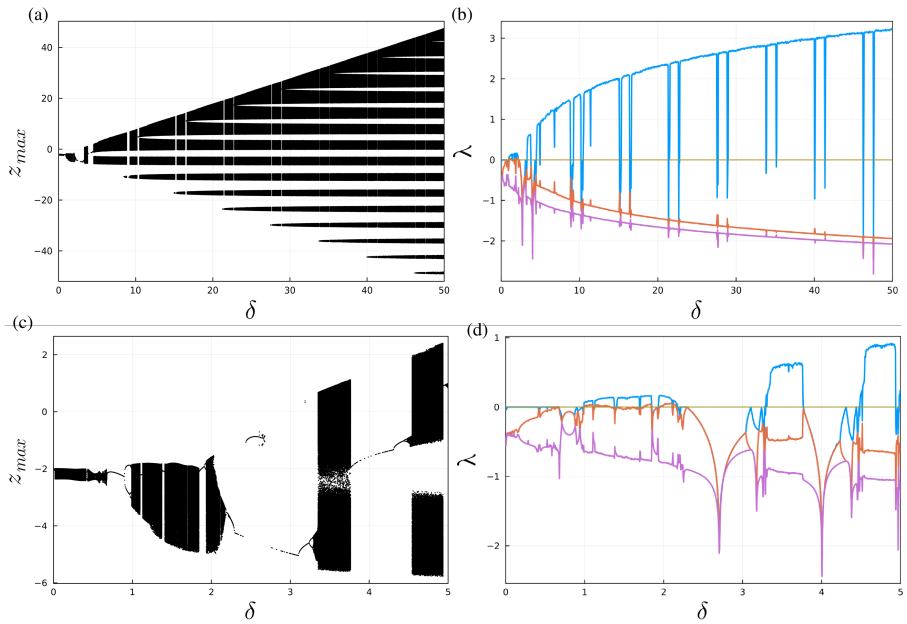

Figure 2. (**a**) Bifurcation diagram as a function of δ, which ranges from 0 to +50, and (**b**) the corresponding Lyapunov exponents (LEs). (**c**,**d**) show a zoomed-in view of a portion of the bifurcation diagram and the associated LEs.

In addition, the local maxima of the z variable are obtained by varying the amplitude of sine function δ in Figure 2. As seen in Figure 2a, increasing the range of δ raises the amplitude of the attractors. We observed that chaotic attractors are interspersed with periodic attractors. To exemplify this, the Lyapunov exponents are depicted in Figure 2b. It is significant to note that chaotic regions show one of the LE takes positive values, but interspersed periodic attractors in the chaotic regions acquire negative LE. For a clearer understanding of the transition, we focused on a small portion of the region near the bifurcation and presented the zoomed-in image in Figure 2c,d. When the bifurcation transition is compared to LE, it is obvious that at smaller values of δ, quasi-periodic attractors exist. Increasing δ leads to the transition from periodic to chaotic attractors via the period doubling route. Further raising the value of δ illustrates alternate manifestations of periodic and chaotic attractors.

In order to examine the impact of feedback strength the bifurcation diagram with the associated LEs are presented in Figure 3a,b by varying μ from negative to positive values. When the feedback strength is negative, we found periodic attractors. We discovered that period doubling facilitates the shift to hyperchaotic attractor with adequate strength positive feedback. The observed periodic to chaotic transitions are validated further through the LEs. Importantly, the existence of a hyperchaotic attractor is supported by the presence of two positive LEs Figure 3b.

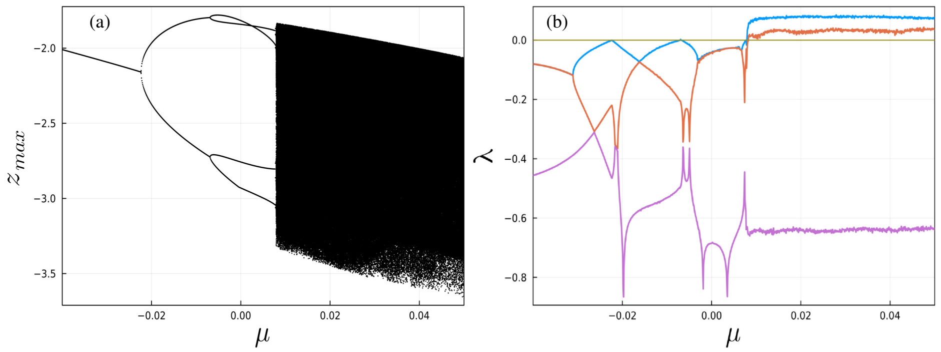

Figure 3. (**a**) Bifurcation diagram as a function of the feedback strength μ, and (**b**) the associated Lyapunov exponents (LEs).

4. Symmetric Patterns in Two Parameter Spaces

To illustrate the global dynamical transitions in the parametric space, we portrayed two parameter diagram in (α, μ) parametric space in Figure 4a. The maximal LE is used to distinguish the dynamical regions, and the color bar indicates the range of LE. For each value of μ, there exists a different symmetric repeating pattern as a function of α. Mainly, we observed two types of transitions in each patch in Figure 4a, which depend on the strength of feedback, which varies from negative to positive. To show this clearly, we plotted the zoomed-in view of the isolated patch from Figure 4a in Figure 4b. At lower feedback values, that is, during negative feedback strength, the transition from periodic $\rightarrow$ chaotic $\rightarrow$ periodic $\rightarrow$ chaotic $\rightarrow$ periodic attractor is observed. A transition from periodic $\rightarrow$ chaotic $\rightarrow$ periodic attractors is observed in the positive feedback region. Certain range of parameters α and μ show the periodic attractors in the middle of the chaotic region.

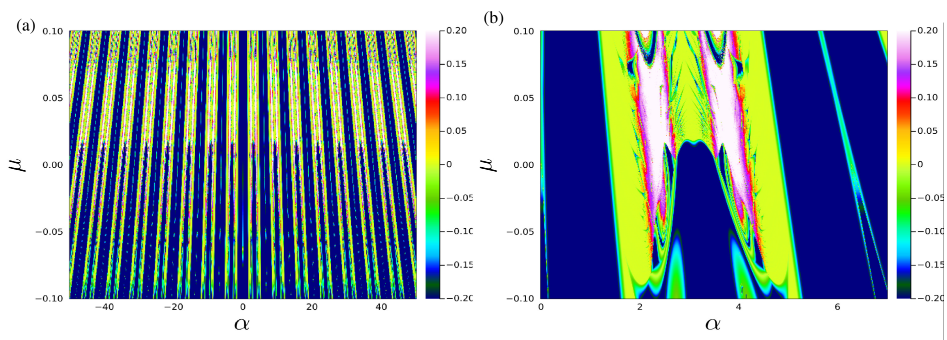

Figure 4. (**a**) The dynamical transitions in (α, μ) parametric space, and (**b**) zoomed-in view of the part of parametric transitions.

Analogously, the dynamical transitions of the system (1) are inspected in (α, δ) parametric space in Figure 5. We can note that the different patches of symmetric pattern with respect to the parameters α and δ (see Figure 5a). To clearly visualize the patterns, the zoomed view of small part is depicted in Figure 5b. It is to be observed the reflection symmetry in the zoomed view left ($\alpha \geq 0$ *or* $\delta \geq 0$) and right ($\alpha \leq 0$ *or* $\delta \leq 0$) sides.

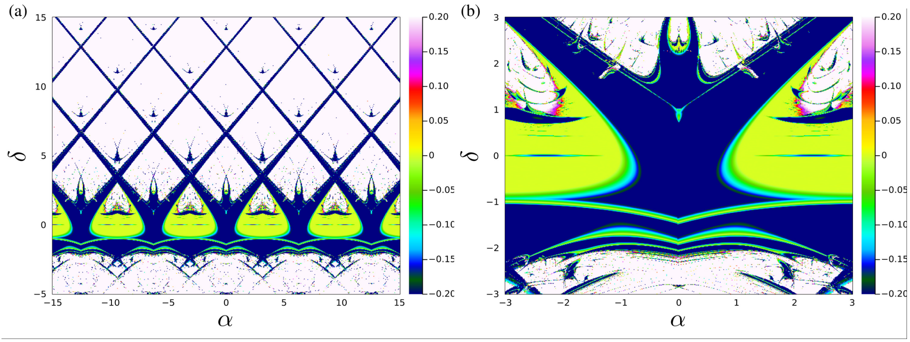

Figure 5. (**a**) The dynamical transitions in (α, δ) parametric space, and (**b**) zoomed-in view of the part of parametric transitions.

5. Dynamical Transitions in Network of Sine Maps

The network dynamics are typically useful in understanding the realistic phenomena observed in many complex systems present in realistic situations. To demonstrate the occurrence of such collective dynamics, we considered a network of sine maps that interact via different complex network connectivities. The expression for a network of sine maps can be written as

$$\begin{aligned} x_{j+1}^k &= y_j^k, \qquad\qquad k,l = 1,2...,N, \\ y_{j+1}^k &= sin(z_j^k), \\ z_{j+1}^k &= \alpha + \beta x_j^k + \gamma y_j^k - \delta sin(z_j^k) + \mu z_j^k + \sigma H(x_j^k, x_j^l), \end{aligned} \tag{2}$$

where, $H(x_j^k, x_j^l) = \frac{1}{N}\sum_{l=1}^{N} A_{kl}(x_j^k, x_j^l)$ is the coupling function and σ is the coupling strength. A_{kl} is the connectivity matrix, if the k^{th} map is connected with l^{th} map or vice versa, then $A_{kl} = 1$, otherwise $A_{kl} = 0$. Primarily the dynamical transitions of the system (2) are investigated for small-world network interactions with the probability $\rho = 0.5$ by fixing the feedback strength as $\mu = -0.05$ and setting different coupling strengths. For coupling strength $\sigma = 0.001$, there exists a two-cluster state as shown in Figure 6(ai). The nodes in the maps are distributed in the two different values is evident from Figure 6(aii). When increasing the strength of coupling, we observed a few of the nodes in the upper cluster shift to the lower clusters as shown in Figure 6(bi,bii) for $\sigma = 0.02$. From Figure 6(ci,cii) and Figure 6(di,dii), it is clear increasing the coupling strength to $\sigma = 0.03$ and $\sigma = 0.04$ shifts the remaining oscillators to the lower branch thereby resulting the number of nodes is decreased in the upper cluster. Finally, all the nodes are settled in one cluster and exhibit the synchronization Figure 6(ei,eii) when the coupling strength is $\sigma = 0.06$.

The dynamical behavior of the system (2) is investigated for regular and small-world network interactions when fixing the coupling strength $\sigma = 0.1$ and varying the strength of self-feedback from negative to positive values. Figure 7(ai,aii) delineates the existence of synchronization behavior if the coupling strength $\sigma = 0.1$ and the feedback strength $\mu = -0.03$. If the strength of feedback is increased to $\mu = -0.01$, the partial nodes in the synchronization state exhibit incoherent behavior while the remaining are in synchronization as in Figure 7(bi). Such hybrid coexisting synchronized and desynchronized states are referred to as chimera states. The desynchronized nodes are distributed randomly while all other nodes are in coherent behaviors is evident from the snapshot Figure 7(bii). Upon increasing the feedback to a positive value ($\mu = 0.01$) give rise to the partial coherent nodes also shifting to the incoherent behavior resulting in entire nodes in the network exhibiting the desynchronization state as depicted in Figure 7(ci,cii).

Following that, the dynamical transitions of the network of sine maps are investigated for small world network interactions ($\rho = 0.5$) in Figure 8. We showed the existence of synchronization state at lower ranges of feedback strength $\mu = -0.05$, as shown in Figure 8(ai,aii). Followed by the transition to desynchronization via chimera state is observed when increasing $\mu = -0.01$ (see Figure 8(bi,bii)), and $\mu = 0.01$ (see Figure 8(ci,cii)). In this manner, the transition from synchronization (coherent) to desynchronization (incoherent) via chimera (coexisting coherent and incoherent) state is identified when raising the strength of feedback. The random network connectivities exhibit a similar kind of dynamical transition (not illustrated here) as the regular and small-world network connectivities.

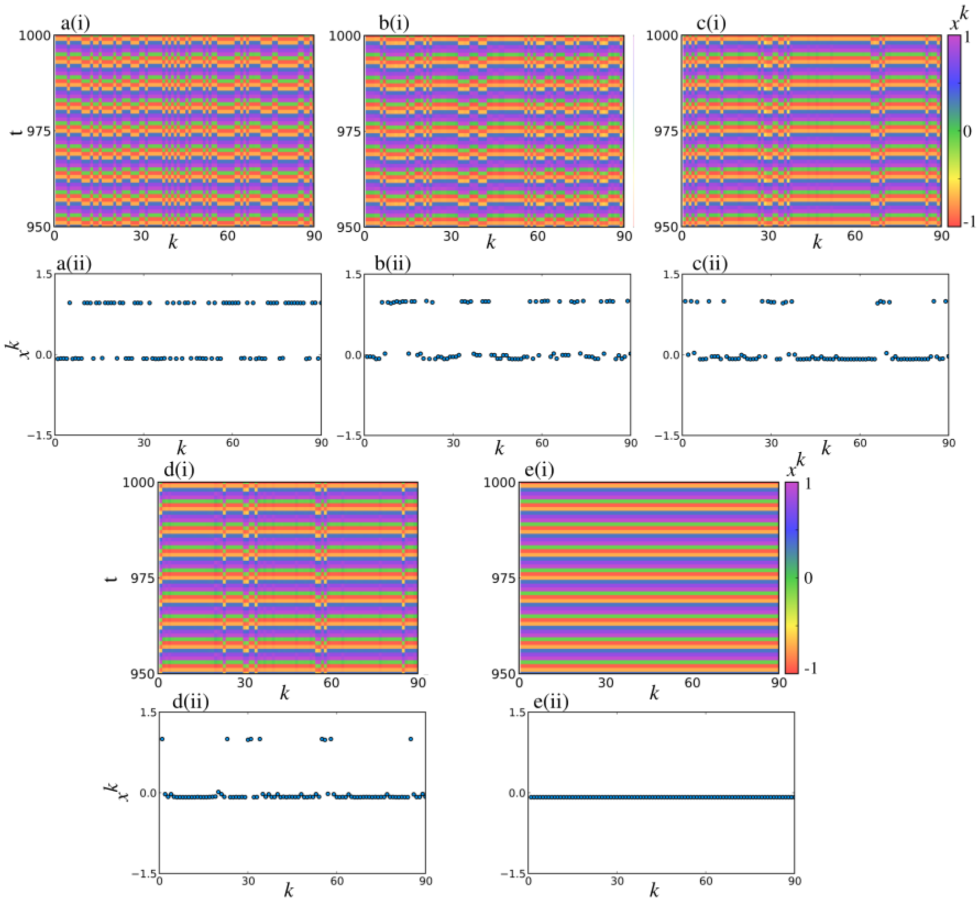

Figure 6. Space-time (i) and the snapshot (ii) images of sine maps networks for small world network $\rho = 0.5$ and by fixing $\mu = -0.05$, (**ai–di**,**aii–dii**) cluster state for $\sigma = 0.001$, $\sigma = 0.02$, $\sigma = 0.03$, $\sigma = 0.04$ and (**ei**,**eii**) synchronization state for $\sigma = 0.06$.

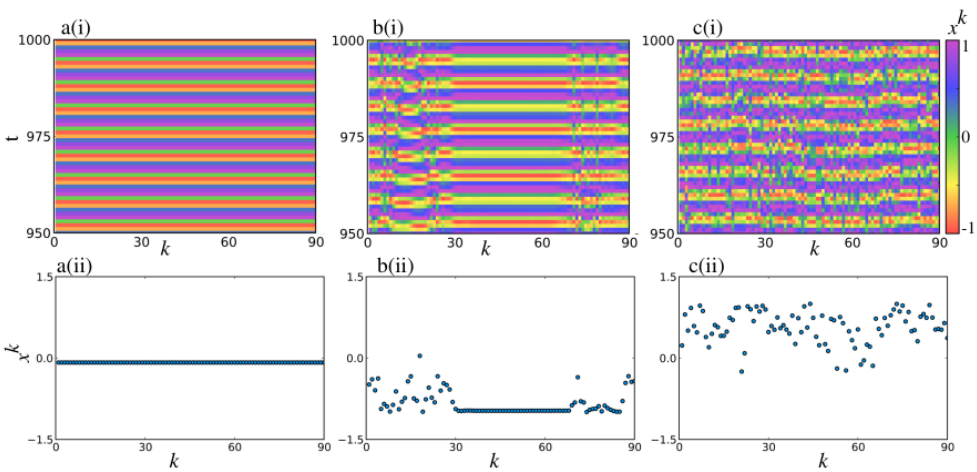

Figure 7. Space-time (i) and the snapshot (ii) images of sine maps networks for regular network $\rho = 0.0$ and by fixing $\sigma = 0.10$, (**ai**,**aii**) synchronization for $\mu = -0.03$, (**bi**,**bii**) chimera for $\mu = -0.01$, and (**ci**,**cii**) desynchronization for $\mu = 0.01$.

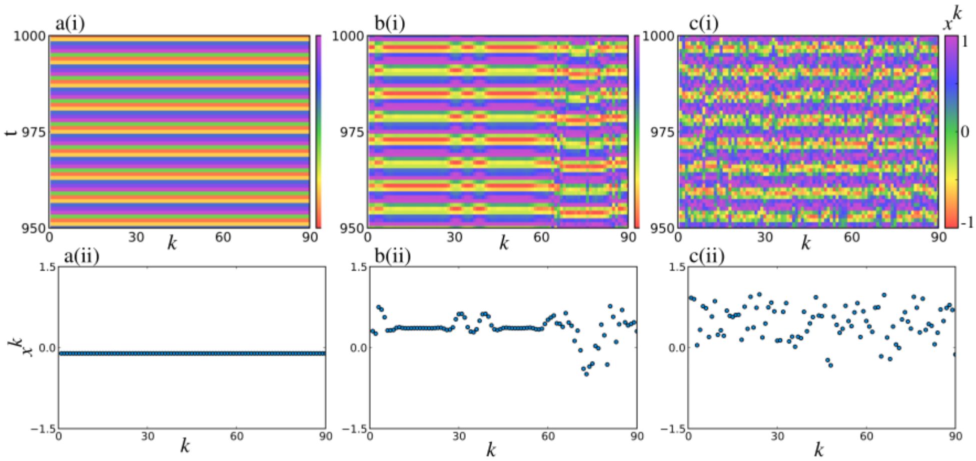

Figure 8. Space-time (i) and the snapshot (ii) images of sine maps networks for small world network $\rho = 0.5$ and by fixing $\sigma = 0.10$, (**ai**,**aii**) synchronization for $\mu = -0.03$, (**bi**,**bii**) chimera for $\mu = -0.01$, and (**ci**,**cii**) desynchronization for $\mu = 0.01$.

6. Conclusions

In this study, a 3D sinusoidal map is considered to understand its dynamical transitions. In addition, we included a self-feedback factor in the considered system to investigate its impact for the first time in the literature. We show that increasing the bifurcation parameter of the systems gives rise to symmetric patterns in the dynamical transitions while shifting between the chaotic and periodic attractors. Then increasing the amplitude of the sine functions can help to enhance the amplitude of the attractors. The impact of the self-feedback factor was also investigated and observed that the existence of hyper chaotic behavior at the sufficient strength of positive self-feedback. The dynamical transitions are pictured in two parametric diagrams using LEs to show the manifestation of symmetric patterns. Interestingly, we found the existence of parametric symmetry while varying the bifurcation parameter with a self-feedback factor or bifurcation parameter with amplitude of sine function. In addition, the analysis is performed by extending the proposed system to the network of coupled sine maps by fixing the feedback strength as constant. For the small-world network, we observed the transition from cluster state to synchronization state as a function of coupling strength. Instead of fixing the coupling strength, varying the magnitude feedback from negative to positive values resulting in the transition from synchronization to desynchronization via chimera state for REG, SW, and RAND network connectivities. We believe that obtained collective dynamics and symmetric patterns can be helpful to realize the occurrence of such patterns observed in physical, biological, and chemical systems.

Author Contributions: Conceptualization, K.R. and S.K.; methodology, K.R., S.K. and A.K.; software, K.R., S.K. and A.K.; validation, K.R., A.K. and C.V.; formal analysis, K.R. and S.K.; investigation, K.R. and S.K.; resources, A.K. and C.V.; data curation, K.R., S.K., A.K. and C.V.; writing—original draft preparation, A.K. and C.V.; writing—review and editing, K.R., S.K., A.K. and C.V.; visualization, K.R., S.K., A.K. and C.V.; supervision, K.R., A.K. and C.V.; project administration, K.R., A.K. and C.V.; funding acquisition, K.R. and C.V. All authors have read and agreed to the published version of the manuscript.

Funding: Center for Nonlinear Systems, Chennai Institute of Technology (CIT), India, Funding Number: CIT/CNS/2023/RP-005 .

Institutional Review Board Statement: Not applicable.

Informed Consent Statement: Not applicable.

Data Availability Statement: Data generated during the current study will be made available at reasonable request.

Acknowledgments: We gratefully acknowledge that this work was funded by the Center for Nonlinear Systems, Chennai Institute of Technology (CIT), India, via funding number CIT/CNS/2023/RP-005.

Conflicts of Interest: The authors declare no conflict of interest.

Sample Availability: Not applicable.

References

1. Tsonis, A.A. *Chaos: From Theory to Applications*; Springer Science & Business Media: Berlin/Heidelberg, Germany, 2012.
2. Broer, H.W.; Takens, F. *Dynamical Systems and Chaos*; Springer: New York, NY, USA, 2011; Volume 172, p. 133.
3. Premraj, D.; Kumarasamy, S.; Thamilmaran, K.; Rajagopal, K. Strange nonchaotic attractor in memristor-based van der Pol oscillator. *Eur. Phys. J. Spec. Top.* **2022**, *231*, 3143–3149. [CrossRef]
4. Durairaj, P.; Kanagaraj, S.; Kathamuthu, T.; Rajagopal, K. Strange Nonchaotic Attractors in Memristor-Based Shimizu–Morioka Oscillator. *Int. J. Bifurc. Chaos* **2022**, *32*, 2230022. [CrossRef]
5. Rajagopal, K.; Kumarasamy, S.; Kanagaraj, S.; Karthikeyan, A. Infinitely coexisting chaotic and nonchaotic attractors in a RLC shunted Josephson Junction with an AC bias current. *Eur. Phys. J. B* **2022**, *95*, 149. [CrossRef]
6. Lorenz, E.N. Deterministic nonperiodic flow. *J. Atmos. Sci.* **1963**, *20*, 130–141. [CrossRef]
7. Sprott, J.C. Some simple chaotic flows. *Phys. Rev. E* **1994**, *50*, R647. [CrossRef] [PubMed]
8. Rössler, O.E. An equation for continuous chaos. *Phys. Lett.* **1976**, *57*, 397–398. [CrossRef]
9. Chen, G.; Ueta, T. Yet another chaotic attractor. *Int. J. Bifurc. Chaos* **1999**, *9*, 1465–1466. [CrossRef]
10. Liu, X.; Mou, J.; Wang, J.; Banerjee, S.; Li, P. Dynamical Analysis of a Novel Fractional-Order Chaotic System Based on Memcapacitor and Meminductor. *Fractal Fract.* **2022**, *6*, 671. [CrossRef]
11. Chen, Y.; Mou, J.; Jahanshahi, H.; Wang, Z.; Cao, Y. A new mix chaotic circuit based on memristor–memcapacitor. *Eur. Phys. J. Plus* **2023**, *138*, 78. [CrossRef]
12. Gong, L.; Deng, C.; Pan, S.; Zhou, N. Image compression-encryption algorithms by combining hyper-chaotic system with discrete fractional random transform. *Opt. Laser Technol.* **2018**, *103*, 48–58. [CrossRef]
13. Ren, L.; Mou, J.; Banerjee, S.; Zhang, Y. A hyperchaotic map with a new discrete memristor model: Design, dynamical analysis, implementation and application. *Chaos Solitons Fractals* **2023**, *167*, 113024. [CrossRef]
14. Lv, M.; Wang, C.; Ren, G.; Ma, J.; Song, X. Model of electrical activity in a neuron under magnetic flow effect. *Nonlinear Dyn.* **2016**, *85*, 1479–1490. [CrossRef]
15. Ma, J.; Wu, F.; Wang, C. Synchronization behaviors of coupled neurons under electromagnetic radiation. *Int. J. Mod. Phys. B* **2017**, *31*, 1650251. [CrossRef]
16. Wang, L.; Cheng, H. Pseudo-random number generator based on logistic chaotic system. *Entropy* **2019**, *21*, 960. [CrossRef]
17. Bahramian, A.; Nouri, A.; Baghdadi, G.; Gharibzadeh, S.; Towhidkhah, F.; Jafari, S. Introducing a chaotic map with a wide range of long-term memory as a model of patch-clamped ion channels current time series. *Chaos Solitons Fractals* **2019**, *126*, 361–368. [CrossRef]
18. Li, C.; Chen, G. Chaos in the fractional order Chen system and its control. *Chaos Solitons Fractals* **2004** , *22*, 549–554. [CrossRef]
19. May, R.M. Simple mathematical models with very complicated dynamics. *Nature* **1976**, *261*, 459–467. [CrossRef]
20. El-Sayed, A.; El-Raheem, Z.F.; Salman, S.M. A new chaotic behavior of a general model of the Henon map. *Adv. Differ. Equations* **2014**, *2014*, 107. [CrossRef]
21. Liu, Y. Discrete chaos in fractional Hénon maps. *Int. J. Nonlinear Sci.* **2014**, 18, 170–175.
22. Liu, X.; Mou, J.; Yan, H.; Bi, X. Memcapacitor-coupled chebyshev hyperchaotic map. *Int. J. Bifurc. Chaos* **2022**, *32*, 2250180. [CrossRef]
23. Richter, H. The generalized Henon maps: Examples for higher-dimensional chaos. *Int. J. Bifurc. Chaos* **2002**, *12*, 1371–1384. [CrossRef]
24. Chen, G.; Mao, Y.; Chui, C.K. A symmetric image encryption scheme based on 3D chaotic cat maps. *Chaos Solitons Fractals* **2004**, *21*, 749–761. [CrossRef]
25. Li, S.; Chen, G.; Mou, X. On the dynamical degradation of digital piecewise linear chaotic maps. *Int. J. Bifurc. Chaos* **2005**, *15*, 3119–3151. [CrossRef]
26. Behnia, S.; Akhshani, A.; Ahadpour, S.; Mahmodi, H.; Akhavan, A. A fast chaotic encryption scheme based on piecewise nonlinear chaotic maps. *Phys. Lett. A* **2007**, *366*, 391–396. [CrossRef]
27. Tutueva, A.V.; Nepomuceno, E.G.; Karimov, A.I.; Andreev, V.S.; Butusov, D.N. Adaptive chaotic maps and their application to pseudo-random numbers generation. *Chaos Solitons Fractals* **2020**, *133*, 109615. [CrossRef]
28. Khennaoui, A.A.; Ouannas, A.; Bekiros, S.; Aly, A.A.; Alotaibi, A.; Jahanshahi, H.; Alsubaie, H. Hidden Homogeneous Extreme Multistability of a Fractional-Order Hyperchaotic Discrete-Time System: Chaos, Initial Offset Boosting, Amplitude Control, Control, and Synchronization. *Symmetry* **2023**, *15*, 139. [CrossRef]
29. Zhang, J. Control Analysis of Stochastic Lagging Discrete Ecosystems. *Symmetry* **2022**, *14*, 1039. [CrossRef]
30. Wei, C.; Li, G.; Xu, X. Design of a new dimension-changeable hyperchaotic model based on discrete memristor. *Symmetry* **2022**, *14*, 1019. [CrossRef]

31. Andrianov, I.; Koblik, S.; Starushenko, G. Transition from discrete to continuous media: The impact of symmetry changes on asymptotic behavior of waves. *Symmetry* **2021**, *13*, 1008. [CrossRef]
32. Horita, T.; Kanamaru, T.; Akishita, T. Stochastic resonance-like behavior in the sine-circle map. *Prog. Theor. Phys.* **1999**, *102*, 1057–1064. [CrossRef]
33. Moysis, L.; Azar, A.T.; Tutueva, A.; Butusov, D.N.; Volos, C. Discrete Time Chaotic Maps With Application to Random Bit Generation. In *Handbook of Research on Modeling, Analysis, and Control of Complex Systems*; IGI Global: Hershey, PA, USA, 2021; pp. 542–582.
34. Li, C.; Ramach, R.D.; Rajagopal, K.; Jafari, S.; Liu, Y. Predicting tipping points in chaotic maps with period-doubling bifurcations. *Complexity* **2021**, *2021*, 9927607. [CrossRef]
35. Gasri, A.; Ouannas, A.; Khennaoui, A.A.; Bendoukha, S.; Pham, V.T. On the dynamics and control of fractional chaotic maps with sine terms. *Int. J. Nonlinear Sci. Numer. Simul.* **2020**, *21*, 589–601. [CrossRef]
36. Kumari, S.; Chugh, R.; Miculescu, R. On the Complex and Chaotic Dynamics of Standard Logistic Sine Square Map. *Analele Univ. Ovidius Constanta-Ser. Mat.* **2021**, *29*, 201–227. [CrossRef]
37. He, P.; Sun, K.; Zhu, C. A novel image encryption algorithm based on the delayed maps and permutation-confusion-diffusion architecture. *Secur. Commun. Netw.* **2021**, *2021*, 6679288. [CrossRef]
38. Al-Saidi, N.M.; Younus, D.; Natiq, H.; Ariffin, M.R.K.; Asbullah, M.A.; Mahad, Z. A new hyperchaotic map for a secure communication scheme with an experimental realization. *Symmetry* **2020**, *12*, 1881. [CrossRef]
39. Peng, Y.; Lan, Z.; Li, W.; Li, Y.; Peng, J. Modeling different discrete memristive sine maps and its parameter identification. *Eur. Phys. J. Spec. Top.* **2022**, *231*, 3187–3196. [CrossRef]
40. Lee, G.; Farhat, N.H. Parametrically coupled sine map networks. *Int. J. Bifurc. Chaos* **2001**, *11*, 1815–1834. [CrossRef]
41. Maistrenko, V.L.; Maistrenko, Y.L.; Mosekilde, E. Chaotic synchronization and antisynchronization in coupled sine maps. *Int. J. Bifurc. Chaos* **2005**, *15*, 2161–2177. [CrossRef]
42. Chatterjee, N.; Gupte, N. Synchronization in coupled sine circle maps. *Phys. Rev. E* **1996**, *53*, 4457. [CrossRef]
43. Das, A.; Gupte, N. Crisis, unstable dimension variability, and bifurcations in a system with high-dimensional phase space: Coupled sine circle maps. *Phys. Rev. E* **2013**, *87*, 042906. [CrossRef]
44. Brugnago, E.L.; Rech, P.C. Chaos Suppression in a Sine Square Map through Nonlinear Coupling. *Chin. Phys. Lett.* **2011** , *28*, 110506. [CrossRef]
45. Pinto, S.E.D.S.; Viana, R.L. Synchronization plateaus in a lattice of coupled sine-circle maps. *Phys. Rev. E* **2000**, *61*, 5154. [CrossRef] [PubMed]
46. Woo, S.J.; Lee, J.; Lee, K.J. Spiral waves in a coupled network of sine-circle maps. *Phys. Rev. E* **2003**, *68*, 016208. [CrossRef] [PubMed]
47. Mammeri, M. Symmetry and Periodic-Chaos in 3-D Sinusoid Discrete Maps. *Bull. Math. Anal. Appl.* **2017**, *9*, 1–8.